Reproducibility of graph metrics of human brain structural networks

Jeffrey T. Duda [1,*], Philip A. Cook [1] and James C. Gee [1]

[1] *Penn Image Computing and Science Laboratory, University of Pennsylvania, Department of Radiology, Philadelphia, PA, USA*

Correspondence*:
Jeffrey T. Duda
Penn Image Computing and Science Laboratory, University of Pennsylvania,
Department of Radiology, 3600 Market Street, Suite 370, Philadelphia, PA, USA,
jtduda@seas.upenn.edu

Neuroinformatics with the Insight ToolKit

ABSTRACT

Recent interest in human brain connectivity has led to the application of graph theoretical analysis to human brain structural networks, in particular white matter connectivity inferred from diffusion imaging and fiber tractography. While these methods have been used to study a variety of patient populations, there has been less examination of the reproducibility of these methods. These graph metrics typically derive from fiber tractography, however a number of tractography algorithms exist and many of these are known to be sensitive to user-selected parameters. The methods used to derive a connectivity matrix from fiber tractography output may also influence the resulting graph metrics. Here we examine how these algorithm and parameter choices influence the reproducibility of proposed graph metrics on a publicly available test-retest dataset consisting of 21 healthy young adults. Network summary measures are examined using the intraclass correlation coefficient (ICC), and the dice coefficient is used to examine overlap of constant density subgraphs.

Keywords: Structure Tractography Connectivity Brain Network Reproducibility Graph

1 INTRODUCTION

Combining magnetic resonance imaging (MRI) of the human brain with graph theory analysis has emerged as a powerful approach to studying large-scale networks of both structural and functional connectivity. In the case of structural connectivity, the use of diffusion weighted MRI and associated fiber tractography methods provide the ability to identify the long-range pathways that connect cortical regions and form a network architecture (Basser et al., 2000; Lazar et al., 2003; Hagmann et al., 2003; **?**). The use of graph theoretical analysis to study the topology of these structural networks has increasingly been used to examine the structural consequences of neurological disorders (Xie and He, 2012; **?**) as well as the relationship between structure and function ().

Previous studies examining the reproducibly of graph-based metrics in functional networks have shown good levels of reproducibly in MEG (Deuker et al., 2009), fMRI using BOLD contrast (Telesford et al., 2010; Braun et al., 2012; Schwarz and McGonigle, 2011; Liang et al., 2012; **?**) and arterial spin labeling (**?**). A number of studies have also examined reproducibly in structural networks, each focusing on various aspects of the complex processing pipeline that is a prerequisite for these measures. These have included studies of diffusion spectrum imaging (Cammoun et al., 2012; Bassett et al., 2011) and high angular resolution diffusion imaging (Dennis et al., 2012). Some studies have examined probabilistic tractography

(Owen et al., 2013; Vaessen et al., 2010). DTI-based studies using deterministic tractography have included the examination of tractography seed density (Cheng et al., 2012), anatomic label density (Bassett et al., 2011), and studies examining a variety of network measures (Cheng et al., 2012; Irimia and Van Horn, 2012). In the paper we constrain our analysis DTI-based deterministic fiber tractography. Within this constraint, we examine multiple algorithms for computing streamlines and their required parameters to examine their influence on the final graph metrics. A set of manually defined cortical parcellations (Klein and Tourville, 2012) is used along with a more common template-based parcellation scheme (**?**). We use freely available data and software to create a framework that facilitates future extensions that may examine additional aspects of the processing as well as the comparison to, or addition of, multiple imaging modalities.

2 MATERIALS & METHODS

2.1 NEUROIMAGING DATA

The Multi-Modal MRI Reproducibility Resource (Landman et al., 2011) provides a publicly available test-retest data set consisting of 21 healthy control subjects (11 males). The mean age is 31.76 ± 9.35 with a range of [22,61]. This data set provides a multitude of MR image types, but here only the T1-weighted anatomical images and diffusion tensor images are examined. T1 INFO. DTI INFO. The Mindboggle dataset provides a population averaged template for this data set and for one time point for each subject, a brain extracted image, and two sets of manually defined cortical labels are provided (Klein and Tourville, 2012).

2.2 ANATOMICAL DATA PREPROCESSING

ANTs volumetric-based cortical thickness estimation pipeline

The N4 tool was used to perform bias correction on each subject's T1 image (**?**). The antsRegistration tool was used to find a deformable mapping between each subject's T1 and the Mindboggle template for later use in anatomical labeling. An intra subject affine registration was used to align each subject's T1 images. Thresholding and a morphological closing was used to obtain a brainmask from the brain extracted T1 images provided by Mindboggle.

For each subject, a set of manually defined cortical labels was available via Mindboggle (Klein and Tourville, 2012). Additionally, the AAL label set (Tzourio-Mazoyer et al., 2002) was also examined as it is a label set often used in both functional and structural studies. Here a template-based approach is used and the antsRegistration tool is used to find a deformable mapping to the Mindboggle template. These template mapping are then combined with the intrasubject mapping to transfer the AAL labels into the DTI space for each time point.

2.3 DIFFUSION DATA PREPROCESSING

An affine registration was then used to align each T1 image to it's corresponding b=0 image that was acquired as part of the DWI sequence. Composing these intrasubject mappings provides the ability to transform labels between T1 and DTI space and between time points for a subject. The intra subject mappings are then used to warp these labels into the DTI space for each time point using nearest neighbor interpolation.

2.4 FIBER TRACTOGRAPHY

The Camino toolkit () is used to calculate diffusion tensor images via a weighted linear fitting (**??**), and is also used to perform the deterministic tractography. The brainmasks defined in anatomical space are warped into DTI space and are used to restrict the tractography to eliminate false positives that could results from streamlines that leave and then reenter the brain. Fractional anisotropy (FA) images are calculated and a tractography seed-map is created by including all voxels with FA of at least 0.2.

One of the primary differences among the various approaches to deterministic tractograpy is the algorithm used to determine the direction that a streamline should proceed from a given point. Here we examine four different approaches:

Table 1. Descriptions and references for graph metrics examined in this study.

Node metrics	Description	Reference
Degree	Number of connections for a node	
Clustering coefficient	Local neighborhood connectivity	(Watts and Strogatz, 1998)
Path length	Average shortest path to all other nodes	(Watts and Strogatz, 1998)
Global efficiency	“Closeness” to all other nodes	(Latora and Marchiori, 2001)
Local efficiency	“Closeness” to local nodes	
Whole-graph metrics		
Small-world		(Watts and Strogatz, 1998)
Synchronizability		(Motter et al., 2005)
Assortativity		(Newman, 2002)
Hierarchy		(Ravasz and Barabási, 2003)
Cost efficiency		(Achard and Bullmore, 2007)
Rich-club coefficient	Degree to which high-degree nodes preferentially inter-connect	(Colizza et al., 2006)
Network similarity measures		
Network overlap		(van Wijk et al., 2010)
Edge overlap	Percentage of common edges in constant density networks	(**?**)

1. Fiber Assignment by Continuous Tracking (FACT) - The primary direction of diffusion (PDD) is followed until the streamline enters a new voxel (**?**).
2. Euler - The PDD is followed for a constant step size (Basser et al., 2000).
3. Rourth-order Runge-Kutta (RK4) - The direction of the step is determined by taking and averaging a weighted series of partial steps (Basser et al., 2000).
4. Tensor Deflection (TenD) - The entire diffusion tensor is used to deect the estimated ber trajectory (Lazar et al., 2003)

2.5 GRAPH GENERATION

For a given set of streamlines, the Camino toolkit is used to generate a connectivity matrix that records how many streamlines connect each pair of regions in a given set of labels.

2.6 NODE METRICS

As we are interested in whole network summary measures, we examine the mean over all nodes for each of the node-metrics listed in table . For more details on the node metrics see (Rubinov and Sporns, 2010). An ITK module named Petiole was created to calculate the desired network measures from the 2D connectivity matrices (**?**). This module incorporates and extends an existing implementation of a graph class (**?**) and provides ITK functions for a variety of graph metrics while using the matlab-based Brain Connectivity Toolkit (**?**) for algorithmic guidance. While many of these metrics inlude implementations for weighted graphs and directed graphs, here we focus on their application to unweighted, undirected graphs.

2.7 WHOLE-GRAPH METRICS

More formulas go here.

Table 2. Formulas for node metrics.

Degree	$K_i = \sum_{j=1}^{n} A_{ij}$
Clustering coefficient	$C_i = 2 * e_i / K_i(K_i - 1)$
Path length	$L = 1/N(N-1) \sum_{ij \in n, i \neq j} d_{ij}$
Global efficiency	$E_{glob} = E(G) = 1/N(N-1) \sum_{i \neq j \in G} 1/d_{ij}$
Local efficiency	$E_{loc} = 1/N \sum_{i \in n} E(G_i)$

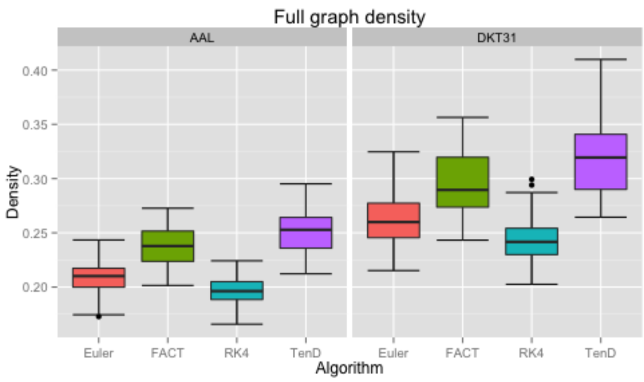

Figure 1. Density

2.8 STATISTICAL ANALYSIS

Dice coefficient for overlap of graph thresholded at a constant density

$$Dice(x, y) = \frac{2\|E(x) \cap E(y)\|}{\|E(x)\| + \|E(y)|}$$

where $E(x)$ is the set of all edges in a graph, x, and edges are considered equal if they connect the same two nodes.

ICC was used to compare the

$$ICC = \frac{\sigma_{bs}^2}{\sigma_{bs}^2 + \sigma_{ws}^2}$$

Permutation testing

3 RESULTS

Overview of what we found

4 DISCUSSION

Other modalities, not examined here, were also acquired making this data useful for future examinations of structure and function.

No smoothing of data here

Other DTI scalar metrics, such as RD, or from other modalities such as MTR.

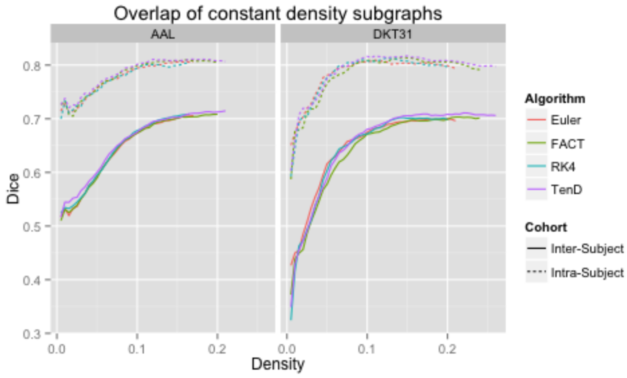

Figure 2. Dice

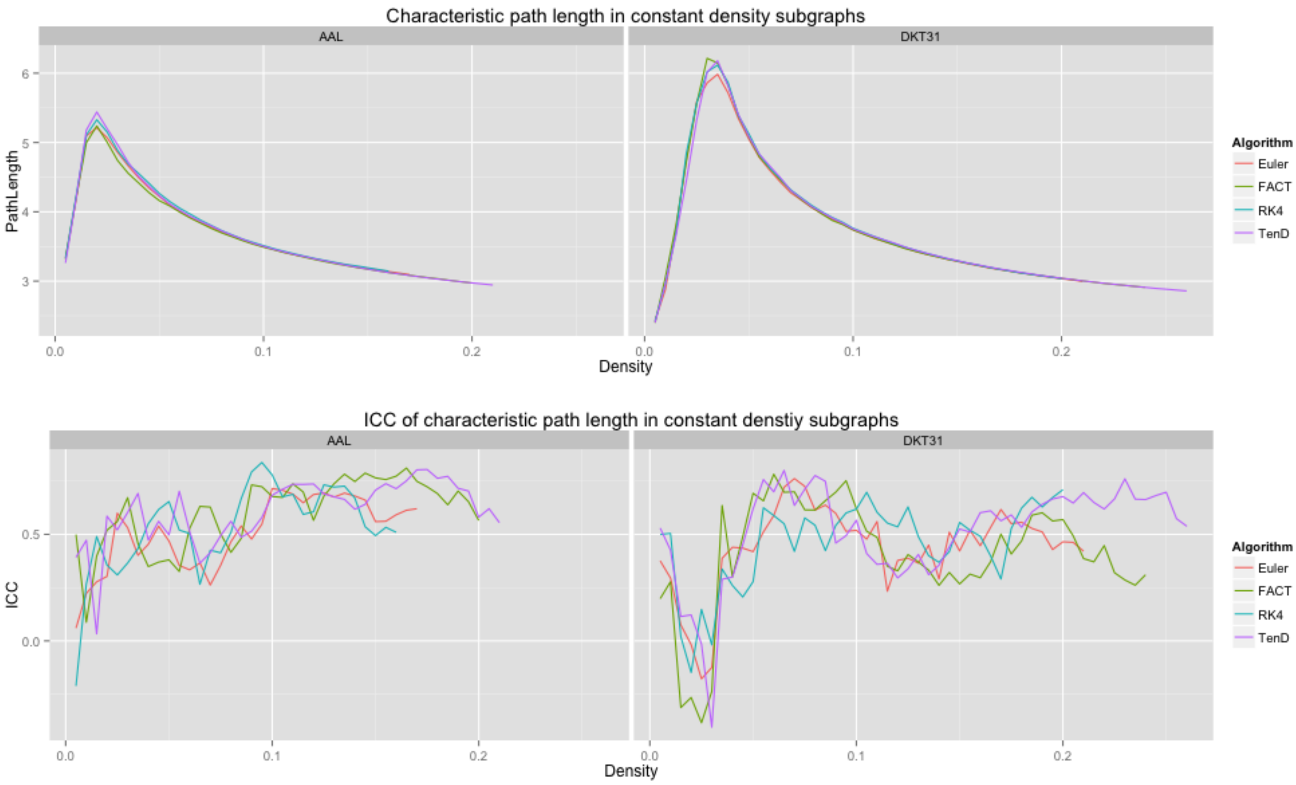

Figure 3. Path

Did not normalize matrices

4.1 DATA SHARING

DISCLOSURE/CONFLICT-OF-INTEREST STATEMENT

The authors declare that the research was conducted in the absence of any commercial or financial relationships that could be construed as a potential conflict of interest.

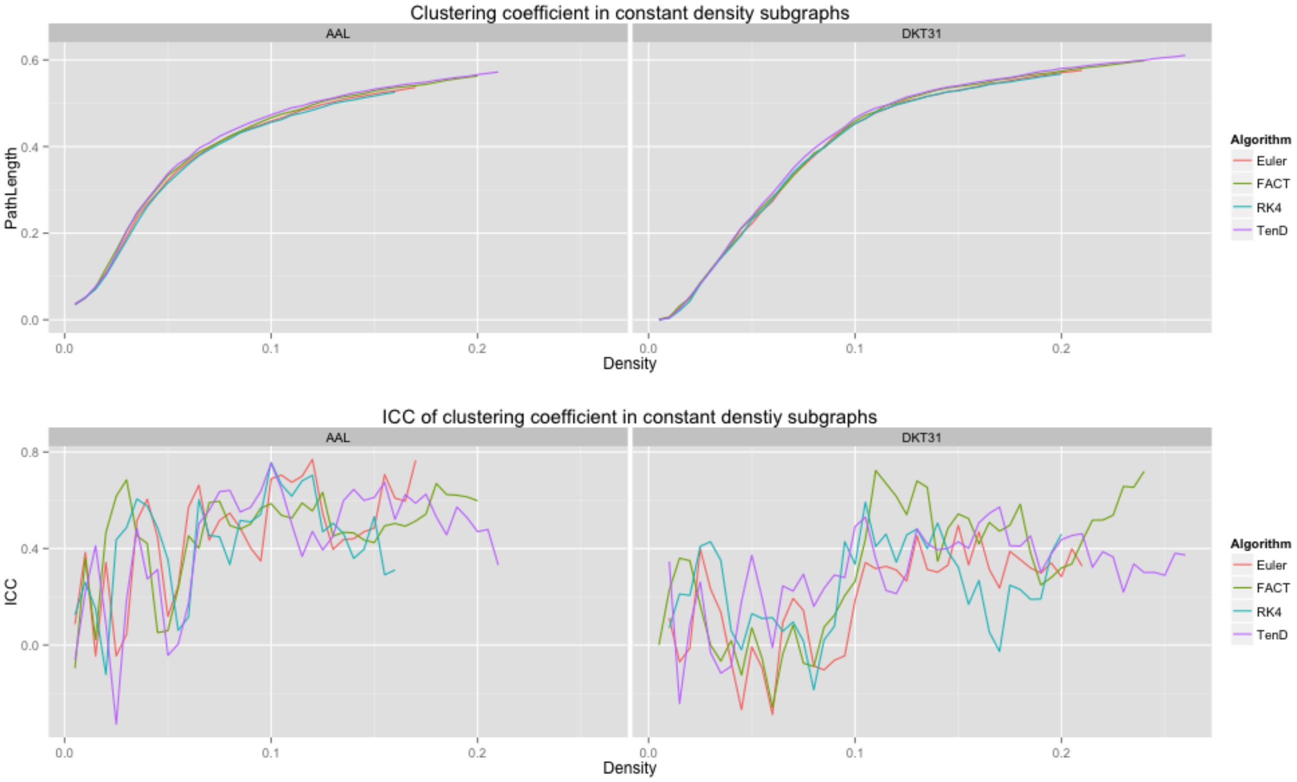

Figure 4. Clust

ACKNOWLEDGEMENT

Shoutouts to our peeps

Funding: Shoutout to our peep$

SUPPLEMENTAL DATA

Maybe need this, maybe not

REFERENCES

Basser, P. J., Pajevic, S., Pierpaoli, C., Duda, J., and Aldroubi, A. (2000) In vivo fiber tractography using dt-mri data. *Magn Reson Med* 44 625–632.

Lazar, M., Weinstein, D. M., Tsuruda, J. S., Hasan, K. M., Arfanakis, K., Meyerand, M. E., et al. (2003) White matter tractography using diffusion tensor deflection. *Hum Brain Mapp* 18 306–321. doi:10.1002/hbm.10102.

Hagmann, P., Thiran, J.-P., Jonasson, L., Vandergheynst, P., Clarke, S., Maeder, P., et al. (2003) Dti mapping of human brain connectivity: statistical fibre tracking and virtual dissection. *Neuroimage* 19 545–554.

Xue, R., van Zijl, P. C., Crain, B. J., Solaiyappan, M., and Mori, S. (1999) In vivo three-dimensional reconstruction of rat brain axonal projections by diffusion tensor imaging. *Magn Reson Med* 42 1123–1127.

Table 3. Functional data analysis is used along with permutation testing to look for pair-wise differences in graph metrics resulting from different fiber tracking algorithms. Only the first time-point for each subject is used. For each metric, the upper-triangular values are for p-values for the AAL labels while the lower-triangular values were generated with the DKT31 labelset.

	Clustering Coefficient				Characteristic Path Length			
	Euler	FACT	RK4	TenD	Euler	FACT	RK4	TenD
Euler		0.2126	0.2716	0.0302*		0.3506	0.1716	0.7984
FACT	0.2734		0.0224*	0.2464	0.5986		0.0344	0.296
RK4	0.8728	0.3434		0.0028*	0.4270	0.7780		0.3064
TenD	0.0604	0.463 0	0.0722		0.9262	0.5958	0.4084	
	Local Efficiency				Global Efficiency			
Euler		0.2126	0.2716	0.0302*		0.3506	0.1716	0.7984
FACT	0.2734		0.0224*	0.2464	0.5986		0.0344	0.296
RK4	0.8728	0.3434		0.0028*	0.4270	0.7780		0.3064
TenD	0.0604	0.463 0	0.0722		0.9262	0.5958	0.4084	

Xie, T. and He, Y. (2012) Mapping the alzheimer's brain with connectomics. *Frontiers in Psychiatry* 2. doi:10.3389/fpsyt.2011.00077.

Deuker, L., Bullmore, E. T., Smith, M., Christensen, S., Nathan, P. J., Rockstroh, B., et al. (2009) Reproducibility of graph metrics of human brain functional networks. *Neuroimage* 47 1460–1468.

Telesford, Q. K., Morgan, A. R., Hayasaka, S., Simpson, S. L., Barret, W., Kraft, R. A., et al. (2010) Reproducibility of graph metrics in fmri networks. *Frontiers in neuroinformatics* 4.

Braun, U., Plichta, M. M., Esslinger, C., Sauer, C., Haddad, L., Grimm, O., et al. (2012) Test–retest reliability of resting-state connectivity network characteristics using fmri and graph theoretical measures. *Neuroimage* 59 1404–1412.

Schwarz, A. J. and McGonigle, J. (2011) Negative edges and soft thresholding in complex network analysis of resting state functional connectivity data. *Neuroimage* 55 1132–1146. doi:10.1016/j.neuroimage.2010.12.047.

Liang, X., Wang, J., Yan, C., Shu, N., Xu, K., Gong, G., et al. (2012) Effects of different correlation metrics and preprocessing factors on small-world brain functional networks: a resting-state functional mri study. *PLoS one* 7 e32766.

Cammoun, L., Gigandet, X., Meskaldji, D., Thiran, J. P., Sporns, O., Do, K. Q., et al. (2012) Mapping the human connectome at multiple scales with diffusion spectrum mri. *J Neurosci Methods* 203 386–397. doi:10.1016/j.jneumeth.2011.09.031.

Bassett, D. S., Brown, J. A., Deshpande, V., Carlson, J. M., and Grafton, S. T. (2011) Conserved and variable architecture of human white matter connectivity. *Neuroimage* 54 1262–1279. doi:10.1016/j.neuroimage.2010.09.006.

Dennis, E. L., Jahanshad, N., Toga, A. W., McMahon, K. L., de Zubicaray, G. I., Martin, N. G., et al. (2012) Test-retest reliability of graph theory measures of structural brain connectivity. *Med Image Comput Comput Assist Interv* 15 305–312.

Owen, J. P., Ziv, E., Bukshpun, P., Pojman, N., Wakahiro, M., Berman, J. I., et al. (2013) Test-retest reliability of computational network measurements derived from the structural connectome of the human brain. *Brain Connect* 3 160–176. doi:10.1089/brain.2012.0121.

Vaessen, M. J., Hofman, P. A. M., Tijssen, H. N., Aldenkamp, A. P., Jansen, J. F. A., and Backes, W. H. (2010) The effect and reproducibility of different clinical dti gradient sets on small world brain connectivity measures. *Neuroimage* 51 1106–1116. doi:10.1016/j.neuroimage.2010.03.011.

Cheng, H., Wang, Y., Sheng, J., Kronenberger, W. G., Mathews, V. P., Hummer, T. A., et al. (2012) Characteristics and variability of structural networks derived from diffusion tensor imaging. *Neuroimage* 61 1153–1164. doi:10.1016/j.neuroimage.2012.03.036.

Irimia, A. and Van Horn, J. D. (2012) The structural, connectomic and network covariance of the human brain. *Neuroimage* 66C 489–499. doi:10.1016/j.neuroimage.2012.10.066.

Klein, A. and Tourville, J. (2012) 101 labeled brain images and a consistent human cortical labeling protocol. *Front Neurosci* 6 171. doi:10.3389/fnins.2012.00171.

Landman, B. A., Huang, A. J., Gifford, A., Vikram, D. S., Lim, I. A. L., Farrell, J. A. D., et al. (2011) Multi-parametric neuroimaging reproducibility: a 3-t resource study. *Neuroimage* 54 2854–2866. doi:10.1016/j.neuroimage.2010.11.047.

Tzourio-Mazoyer, N., Landeau, B., Papathanassiou, D., Crivello, F., Etard, O., Delcroix, N., et al. (2002) Automated anatomical labeling of activations in spm using a macroscopic anatomical parcellation of the mni mri single-subject brain. *Neuroimage* 15 273–289. doi:10.1006/nimg.2001.0978.

Watts, D. J. and Strogatz, S. H. (1998) Collective dynamics of 'small-world' networks. *Nature* 393 440–442. doi:10.1038/30918.

Latora, V. and Marchiori, M. (2001) Efficient behavior of small-world networks. *Physical review letters* 87 198701.

Motter, A. E., Zhou, C., and Kurths, J. (2005) Enhancing complex-network synchronization. *EPL (Europhysics Letters)* 69 334.

Newman, M. E. (2002) Assortative mixing in networks. *Physical review letters* 89 208701.

Ravasz, E. and Barabási, A.-L. (2003) Hierarchical organization in complex networks. *Physical Review E* 67 026112.

Achard, S. and Bullmore, E. (2007) Efficiency and cost of economical brain functional networks. *PLoS Comput Biol* 3 e17. doi:10.1371/journal.pcbi.0030017.

Colizza, V., Flammini, A., Serrano, M. A., and Vespignani, A. (2006) Detecting rich-club ordering in complex networks. *Nature physics* 2 110–115.

van Wijk, B. C. M., Stam, C. J., and Daffertshofer, A. (2010) Comparing brain networks of different size and connectivity density using graph theory. *PLoS One* 5 e13701. doi:10.1371/journal.pone.0013701.

Rubinov, M. and Sporns, O. (2010) Complex network measures of brain connectivity: uses and interpretations. *Neuroimage* 52 1059–1069. doi:10.1016/j.neuroimage.2009.10.003.